

Complementarity between term-time forcing and delayed vaccination response in explaining irregular dynamics in childhood diseases

John C. Eckalbar¹ · Walter L. Eckalbar²

Received: 6 July 2016 / Revised: 10 July 2017 / Published online: 5 February 2018
© Università degli Studi di Napoli "Federico II" 2018

Abstract This paper investigates an *SIR* model with the following properties: (i) demographics are present. (ii) The fraction vaccinating at any time is dependent on past levels of disease prevalence with distributed delay. (iii) The maximum fraction vaccinating is bounded below one by medical contraindications or unshakeable beliefs among a sub-set of the population that the vaccination is not beneficial. (iv) Disease transmissibility is higher when school is in session than when it is not. Our main findings are that the time series of prevalence can exhibit irregular inter-epidemic intervals, and the profile of outbreaks can be highly variable over time—sometimes exhibiting single large peaks and sometimes clusters of closely-spaced lesser peaks.

Keywords Epidemic · *SIR* · Vaccination · Distributed delay · Term-time forcing

Mathematics Subject Classification 34H10 · 65P20

1 Introduction

Relatively simple epidemiological models typically either: (i) converge without oscillation to a disease-free equilibrium, (ii) spiral into an endemic equilibrium from most initial points, or (iii) move away from most initial points near either equilibria toward a periodic orbit. It has long been noted that historical disease data does not suggest that any of the above are typical. (See Brauer et al. [1] and Manfredi and d’Onofrio

✉ John C. Eckalbar
jeckalbar@csuchico.edu

¹ Department of Economics, California State University, Chico, CA 95926, USA

² Lung Biology Center and Department of Medicine, University of California, San Francisco, San Francisco, CA 94143, USA

[2].) Many researchers, both theoretical and empirical, have introduced “extensions” to the simple models to explain observed irregular periods and amplitudes in disease outbreaks.

There have been many avenues of approach, including the introduction of: (i) age structure, following Schenzle [3], Bolker and Grenfell [4], Bolker [5]; (ii) sinusoidal seasonal forcing, which began in 1929 with the work of Soper [6] and is still active today in the work of Bartlett [7], Bailey [8], Aron and Schwartz [9], Acedo et al. [10], Billings and Schwartz [11], Katriel and Stone [12]; (iii) school term-time forcing, Earn et al. [13], Keeling et al. [14], Rohani et al. [15], Olinky et al. [16], Diedrichs et al. [17]; (iv) stochasticity, Bartlett [7], Zhao [18]; and delays from various sources, including (v) vaccination demand responding with delay to outbreaks, Buonomo et al. [19,20], d’Onofrio et al. [21,22]; (vi) vaccination giving temporary immunity, with recovered returning to susceptibility after delay, Greenhalgh et al. [23], and (vii) changes in peoples’ contact rates in response to the history of disease prevalence, d’Onofrio and Manfredi [24]. See [1,2] for a more extensive review.

Researchers working on both sinusoidal seasonal forcing and discrete school-related term-time forcing models have found that irregular periods/amplitudes can exist when the forcing is strong, e.g., transmissibility must be much higher when school is in session than when it is not [4,11,12,14,15]. At the same time, simple distributed delay models including vaccination demand based on past prevalence with “weak” Erlangian kernels do not appear to give rise to irregular dynamics, though higher order Erlang functions (or discrete delay systems) can produce chaos when delay is long [25,26]. Hence, either model extension can yield exotic dynamics, but only with strong forcing or long delay. In the present paper we are interested in combining discrete school-related term-time forcing with high order distributed delay between disease outbreaks and the vaccination demand to see if a model containing both effects yields irregular dynamics with more moderate levels of forcing strength and delay.

We are not the first to examine a *SIR* model with delay and temporal forcing. In 2009 d’Onofrio and Manfredi [24] modeled a *SIR* system where the contact rate is influenced by past levels of disease prevalence, and they mention at the end that chaos was found when sinusoidal seasonal forcing is attached to the resulting contact rate. And in 2013, d’Onofrio, Manfredi, and Salinelli [27] modelled a *SIR* system employing several different means of linking current vaccinations to past values of prevalence and with the contact rate incorporating sinusoidal forcing, noting “how complex the interplay between infection transmission and vaccinating behaviour might be” [2, p. 287]. We see our present work as an extension of the two previously mentioned papers [24,27] to discrete term-time forcing and high-order distributed delay. Our main finding is that when both delay and term-time forcing are included in an *SIR* model, irregular dynamics occur with much lower values of both term-time forcing strength and delay duration.

In Sect. 2, we describe the *SIR* model used and give some general results. In Sect. 3, we look at equilibrium and stability issues. Section 4 contains numerical results. We explore a pure term-time forcing model in Sect. 4.1 and a pure delay model in 4.2. These provide a baseline for Sect. 4.3, in which we activate both factors and find irregular dynamics with moderate forcing strength and more reasonable mean delay durations. Section 5 offers conclusions.

2 The model

The general topic of temporal forcing has been studied for years in mathematical epidemiology. There are two main branches: sinusoidal forcing and term-time forcing. Sinusoidal forcing has been studied extensively [6–12]. In sinusoidal forcing models, we see equations for the transmission term at time t , $\lambda(t)$, typically in the form $\lambda(t) = \lambda_0(1 + \lambda_1 \cos(\frac{2\pi}{365}t))$, for an annual forcing with t measured in days. This would be the natural way to include effects from mean area temperature, hours of daylight, and other smooth events which repeat annually. The second branch of temporal forcing is typically called “term-time forcing,” and it generally employs a step function, like $f(t)$ below, to model the contact rates, with high rates when school is in session and low rates when it is not [3, 13–17].

In the following formulation, time, t , is continuous, and the model is calibrated in days. We assume that $t = 0$ occurs on the first moment of the first day of the first (arbitrarily chosen) reference year. We further assume that a year is exactly 365 days long. If we let $\llbracket x \rrbracket$ denote the largest integer less than or equal to x , then $\llbracket \text{mod}(t + 1, 365) \rrbracket$ maps all t onto the set of integers between 1 and 365. To illustrate: if $t = 17.65$, $\text{mod}(t + 1, 365) = 18.65$, and we are 65% of the way through day 18 in first year; and 950 years later, when $t = 346,768$, we are again in the 18th day of the year. It is handy to have a notation signifying the day of the year. We will use $T \in \{1, 2, \dots, 365\}$. Subscripts under T will denote specific days of interest. Our term-time forcing function is given as follows:

$$f(t) = \begin{cases} \lambda_2 & \text{if } \text{mod}(t + 1, 365) \in [T_{Sb}, T_{Se}] \cup [T_{Fb}, T_{Fe}] \\ \lambda_1 & \text{if } \text{mod}(t + 1, 365) \notin [T_{Sb}, T_{Se}] \cup [T_{Fb}, T_{Fe}] \end{cases}.$$

The function f assigns either the disease transmission value λ_1 or λ_2 to every value of t , depending upon whether or not school is in session. We assume that the Spring school term is in session between the days of the year T_{Sb} and T_{Se} and Fall term is in session between T_{Fb} and T_{Fe} . When school is in session, the transmission term is λ_2 . When school is not in session, the transmission term is λ_1 . Weekends during the school term are counted as school time. For convenience, we assume, $0 < T_{Sb} < T_{Se} < T_{Fb} < T_{Fe} < 365$. Be sure to note that t is a continuous real variable increasing smoothly as time advances, while T is taken from the sub-set of the natural numbers between 1 and 365 designating to the day of the year.

The term-time forcing function is now embedded in an *SIR* model of childhood vaccination, where the vaccination uptake rate follows prior levels of disease prevalence with distributed delay. This follows Buonomo et al. [19, 20] and d’Onofrio et al. [21, 22].

$$\begin{aligned} \frac{dS(t)}{dt} &= bN - bN \min[k_1 + k_2 \frac{1}{N} \int_0^\infty I(t - \tau)G(\tau)d\tau, V_m] - f(t) \frac{S(t)I(t)}{N} - bS(t) \\ \frac{dI(t)}{dt} &= f(t) \frac{S(t)I(t)}{N} - \gamma I(t) - bI(t) \\ \frac{dR}{dt} &= \gamma I(t) + bN \min[k_1 + k_2 \frac{1}{N} \int_0^\infty I(t - \tau)G(\tau)d\tau, V_m] - bR(t). \end{aligned} \tag{System 1}$$

S , I , and R give the number of persons in the susceptible, infectious and recovered classes, respectively. $N = S + I + R$ is the population size. It is easy to verify that N is fixed, so we can drop R from the dynamic analysis, solving for R whenever interested by using $R = N - S - I$. Parameter b is the birth rate; γ is the recovery rate; k_1 is the fraction that vaccinates regardless of past levels of prevalence; k_2 determines (in part) the size of the endogenous vaccination response to past prevalence; and V_m is a limiting value on the fraction of newborns that can (or will) vaccinate. The function $G(\tau)$ comes about as follows: One can imagine different individuals with varying personal delay durations ($\tau_i, \tau_j, \text{etc.}$) between a disease outbreak and their vaccination responses. These differences may be due to the dissimilarities in the timeliness of their receipt of information on outbreaks of disease, their personal risk assessments, proclivity to procrastinate, and many other factors. $G(\tau)$ is the probability distribution characterizing the array of personal delay times over the whole population. The expression $\int_0^{\infty} I(t - \tau)G(\tau)d\tau$ in the above set of integro-differential equations has $G(\tau)$ assigning weights to all past levels of disease prevalence according to how long ago (τ) that prevalence level existed. We assume that $G(\tau)$ is an Erlang function, which is given by

$$G(\tau) = \frac{a^n \tau^{n-1} e^{-a\tau}}{(n-1)!}.$$

Here, τ is a delay interval, e is the base of the natural logs, n is a positive integer called the “shape” parameter, and a is a positive number often called the “rate.” Parameters a and n determine the position of the distribution. The mean delay is given by n/a , and the standard deviation is \sqrt{n}/a . The coefficient of variation, the ratio of the standard deviation to the mean, is then given by $1/\sqrt{n}$. Thus, n determines the concentration about the mean.

For concreteness, Fig. 1 plots three different Erlang specifications with the same mean delay, 90 days. We use $n = 1, 3$, and 64 , adjusting parameter a to ensure $n/a = 90$. In the case of $n = 1$, Erlang reduces to an exponential distribution, $G(\tau) = ae^{-a\tau}$. In this case, we have $G(0) = a > 0$, and $G'(\tau) < 0$. Thus, today’s prevalence has the largest impact on today’s vaccination uptake, and the longer the delay (the larger is τ), the smaller is the influence on vaccination. Ruan [28] has referred to these models as having a “weak kernel,” and the $n = 1$ case is also often described as displaying “fading memory.” As n rises above one, the Erlang distribution becomes more Gaussian-looking and is more tightly packed around the mean. Further, when $n > 1$, the current state of I has no impact on current vaccination, since $G(0) = 0$ for all $n > 1$. When $n \rightarrow \infty$, the Erlang distributed delay system approaches the discrete delay formulation.

Our preference in modelling the delayed response of vaccination to past prevalence is to employ $n > 1$. If it takes time for people to recognize that a disease outbreak is underway, and more time to respond by obtaining a vaccination, then we would rather not use the $n = 1$ case, where $G(0) > 0$. Almost all of what follows uses $n = 3$ or $n = 64$. From a theorist’s point of view, it is significant that as n increases from one, the delay system quickly gets very challenging to analyze. Numerically, this

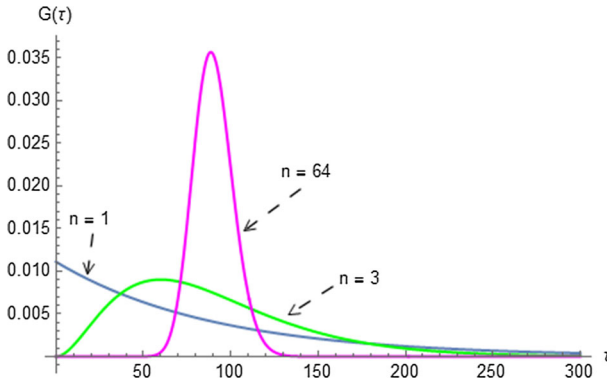


Fig. 1 This shows three Erlang distributions, all with mean delay of 90 days. The values of n are shown in the figure, and parameter a is adjusted to ensure that n/a (mean delay) is 90

is not an insurmountable problem (though the programming and machine time grow), but analytically the challenge is daunting. The $n = 1$ case (“weak kernel or fading memory”) has been thoroughly studied in the context of delayed vaccination response to disease outbreaks, though discrete school-related term-time forcing is not present in the models. See Buonomo et al. [19,20] and d’Onofrio et al. [21,22]. In the interest of linking with those results, we do look briefly at the $n = 1$ case with moderate levels of delay and term-time forcing. The result, as we will see, can be chaos.

Thanks to the work of MacDonald [29], System (1) can be reduced, *via* the so-called “linear chain trick,” to the ordinary differential equations shown here:

$$\begin{aligned}
 dI(t)dt &= f(t) \frac{S(t)I(t)}{N} - \gamma I(t) - bI(t) \\
 dY_0(t)dt &= a(I(t) - Y_0(t)) \\
 dY_j(t)dt &= a(Y_j(t) - Y_{j+1}(t)) \quad j = 0, 1, \dots, n - 1 \\
 dS(t)dt &= bN - bN \min[k_1 + k_2 \frac{Y_{n-1}(t)}{N}, V_m] \\
 &\quad - f(t) \frac{S(t)I(t)}{N} - bS(t).
 \end{aligned}
 \tag{System 2}$$

The Y terms here are synthetic variables. See Smith [30]. Note that the fraction vaccinating at time t , which we call $V(t)$, is given by $V(t) = \min[k_1 + k_2 \frac{Y_{n-1}(t)}{N}, V_m]$.

System (2) is a hybrid dynamical system, where the differential equation driving S and I (and the synthetic variables) switch for two different types of reasons: (1) There is term-time forcing where $f(t)$ switches the transmission term between λ_1 and λ_2 four times per year. (2) The \min function in the dS/dt equation means that the rate of change in S is sometimes governed by V_m and sometimes by Y_{n-1} , depending upon the state of the system. These issues, together with the relatively high dimensionality of the system, present serious obstacles to a complete general analysis, as has been noted by many others working in this general area [3,4,10,14].

3 Equilibria and stability

Before we begin the equilibrium/stability analysis, we will collect a few assumptions. First, there are standard sign restrictions for these sorts of models

$$b, \lambda_1, \lambda_2, \gamma, k_1, k_2, a, n, N, V_m > 0, \quad (\text{A1})$$

to which we add

$$\lambda_1 \leq \lambda_2, \quad k_1 < V_m \leq 1, \quad V_m < V_m^*. \quad (\text{A2})$$

The assumption that $\lambda_1 \leq \lambda_2$ means that the transmission rate during the school term is (at least weakly) higher than when school is out. Since k_1 is the fraction of newborns vaccinating regardless of the past prevalence, and V_m is the maximum possible vaccination fraction, we get $k_1 < V_m \leq 1$. The inequality $V_m < V_m^*$ rules out a type of endemic equilibrium where vaccination is at its ceiling value. We leave this possibility aside for reasons of space. (See [25, 26] for coverage.)

Let us define the weighted transmission rate $\lambda_w = w_1\lambda_1 + w_2\lambda_2$, where $w_2 = (T_{Se} - T_{Sb} + T_{Fe} - T_{Fb})/365$ and $w_1 = 1 - w_2$. Thus, λ_w combines λ_1 and λ_2 , weighing each according to how many days it applies over the year. We also define quasi-basic reproduction numbers:

$$R_0(\lambda_w) = \frac{\lambda_w}{b + \gamma} \quad \text{and} \quad (1)$$

$$R'_0(\lambda_w) = \frac{\lambda_w(1 - k_1)}{b + \gamma}. \quad (2)$$

Equation (1) applies to systems without vaccination and (2) takes account the fixed fraction vaccinating. We use $R_0(\lambda_w)$ and $R'_0(\lambda_w)$, not to explain system behavior, but to constrain us as we consider various combinations of λ_1 and λ_2 . For instance, if we fix values for T_{Se} , T_{Sb} , T_{Fe} , and T_{Fb} , and if we assume $R_0(\lambda_w) = 16$, when we pick a value for λ_2 , the value for λ_1 is implied, since λ_w is a convex combination of λ_1 and λ_2 . We further assume both $R_0(\lambda_w) > 1$ and $R'_0(\lambda_w) > 1$. Our intent is to study systems where the disease persists. Finally, it is sometimes convenient to express λ_2 as a multiple of λ_1 . Thus, we define $m = \lambda_2/\lambda_1$.

3.1 Disease-free equilibrium

System (2) will always have a disease-free equilibrium, E_0 . This is easily seen by setting I and all the time derivatives to zero. Holding notation down by assuming $n = 3$, the result is:

$$E_0 = (S_0, I_0, Y_{0,0}, Y_{1,0}, Y_{2,0}) = (N(1 - k_1), 0, 0, 0, 0),$$

where, for example, $Y_{1,0}$ gives the disease-free equilibrium value for Y_1 .

Note that any equilibrium must have $I = Y_0 = Y_1 = Y_2$. When we feel that no confusion will result, we will write E_0 simply using $(S_0, I_0) = (N(1 - k_1), 0)$. Note that the term-time forcing presents no obstacle with respect to the determination of E_0 , since the same values for S_0 and I_0 result, regardless of whether school is in session or not, i.e., as far as the value of the E_0 equilibrium is concerned, λ_1 and λ_2 play no role.

Stability of E_0 is more complicated, however. Suppose that instead of $f(t)$ in System (2), we had either λ_1 or λ_2 , but no term-time switching. Referring to either λ_1 or λ_2 as λ_i , this specification will be defined as the “pure λ_i sub-system” of System (2). Then it is not hard to show (see [25], Theorem 1) that the Jacobian of System (2) evaluated at E_0 would be

$$J(E_0) = \begin{pmatrix} -b - \gamma + (1 - k_1)\lambda_i & 0 & 0 & 0 & 0 \\ a & -a & 0 & 0 & 0 \\ 0 & a & -a & 0 & 0 \\ 0 & 0 & a & -a & 0 \\ -(1 - k_1)\lambda_i & 0 & 0 & -bk_2 & -b \end{pmatrix},$$

and the eigenvalues would be $-a$ (multiplicity 3), $-b$, and $-b - \gamma + \lambda_i(1 - k_1)$. Clearly, E_0 would be stable if $-b - \gamma + \lambda_i(1 - k_1) < 0$. If we define $R'_0(\lambda_i) = \frac{\lambda_i(1 - k_1)}{b + \gamma}$, then $-b - \gamma + \lambda_i(1 - k_1) < 0$ is equivalent to $R'_0(\lambda_i) < 1$. Under our assumptions that $R'_0(\lambda_w) > 1$ and λ_w is a convex combination of λ_1 and λ_2 , both of the $R'_0(\lambda_i)$ cannot be less than 1. But with $m(:= \lambda_2/\lambda_1)$ sufficiently large, meaning $m > (R'_0(\lambda_w) - w_1)/(1 - w_1) := m_c$, we can get $R'_0(\lambda_1) < 1$ and $R'_0(\lambda_2) > 1$. If this is the case, then under the hybrid given by System (2), during vacations the system would move on a path that would *ultimately* take it arbitrarily close to the disease-free equilibrium, *if the vacation period did not end*; but before the path could get to E_0 , school would re-start and the path would abandon the approach to E_0 and come under the influence of the pure λ_2 sub-system, which does not approach E_0 . The end result is:

Theorem 1 *Unless the hybrid System (2) has an initial point with $I = 0$, if $R'_0(\lambda_w) > 1$, it cannot converge to a disease-free equilibrium*

Hybrid systems are capable of strange things. Two stable sub-systems can “paste together” forming a hybrid that is unstable, and two unstable sub-systems can join to form a stable hybrid system. See Branicky [31] for an introduction. As we see next, the hybrid System (2) will have no endemic equilibria at all.

3.2 Endemic equilibria

Our assumption that $R'_0(\lambda_w) > 1$, forces $R'_0(\lambda_2) > 1$. For sufficiently small values of m , meaning $m < m_c$, we also have $R'_0(\lambda_2) > 1$. We look at this case now. A pure λ_i sub-system would have an endemic equilibrium given by

$$E_1(\lambda_i) = (S_1(\lambda_i), I_1(\lambda_i)) = \left(\frac{N(b + \gamma)}{\lambda_i}, \frac{bN(-b - \gamma + \lambda_i(1 - k_1))}{\lambda_i(b(1 + k_2) + \gamma)} \right) \quad i = 1, 2.$$

Notice that $I_1(\lambda_i) = \frac{bN(R'_0(\lambda_i)-1)}{\lambda_i(b(1+k_2)+\gamma)}$, so $I_1(\lambda_i) > 0$ if and only if $R'_0(\lambda_i) > 1$. In the case under consideration, both pure sub-systems will have endemic equilibria. In contrast with the pure λ_1 or λ_2 sub-systems, the full hybrid System (2) is periodically turning one sub-system off and another on *via* $f(t)$. When $f(t)$ turns on a sub-system, say, the λ_2 sub-system, the flow will temporarily go toward, away from, or around $E_1(\lambda_2)$, depending on the stability properties of $E_1(\lambda_2)$ in the λ_2 sub-system. In a sense, $E_1(\lambda_i)$ is relevant in the hybrid, but it is not an equilibrium. Some authors call it a “ghost” (Crommelin [32]) or “phantom” equilibrium. That is because, even if the hybrid system were to arrive at $E_1(\lambda_2)$, when $f(t)$ switches the active sub-system (with $\lambda_1 \neq \lambda_2$), the path leaves $E_1(\lambda_2)$. It is not a “rest point.” Still, it can be handy to think of the flow of the hybrid in light of the positions and properties of these phantom equilibria. The result of this section is:

Theorem 2 *If $m > m_c$, both pure sub-systems have “phantom” endemic equilibria, but there is no endemic equilibrium for the hybrid system.*

Not all the news is odd, however. Using hybrid System (1), it is not hard to show:

Theorem 3 *If the initial conditions $(S(0), I(0))$ are in the closed bounded set $\Omega = \{(S, I) | S, I \geq 0, S + I \leq N\}$, then the positive semi-path from that point remains in Ω .*

Proof We check the flow of System (1) on the border of Ω and verify that it is never outward. (i) If $S = 0$, $dS/dt = bN - bN \min[k_1 + k_2 \frac{1}{N} \int_0^\infty I(t - \tau)G(\tau)d\tau, V_m] > 0$, since $\min[\dots]$ is a positive fraction. (ii) If $I = 0$, $dI/dt = 0$. (iii) If $S + I = N$, then R must be zero. If so, the last line of System (1) shows that dR/dt is positive, which causes $S + I$ to fall. □

To summarize this section so far: We see that unless the initial value is E_0 , we can expect positive semi-paths to always be moving in Ω . We might see relatively simple periodic orbits or chaos, but not convergence to an equilibrium unless $I(0) = 0$ and the path slides toward E_0 . Also, since System (1) does not have a continuous vector field, we do not have access to the Poincare-Bendixson theorem, and we cannot be surprised to see a positive semi-path crossing itself as time advances. A segment of the path driven by the λ_1 pure sub-system will not cross another segment driven by the same sub-system, but it can cross a segment driven by the λ_2 pure sub-system, and *vice versa*.

We end this section with one more general result that is useful in the following section. The stability of the pure λ_i sub-systems is easy to check numerically using results from [25]. Employing Routh–Hurwitz, Lienard–Ghipart, and the assumptions here, $E_1(\lambda_i)$ is stable in the pure λ_i sub-system iff $det(H_4) > 0$, where $det(H_4) = c_1c_2c_3c_4 - c_3^2c_4 - c_1^2c_4^2 - c_1c_2^2c_5 + c_2c_3c_5 + 2c_1c_4c_5 - c_5^2$, and

$$\begin{aligned} c_1 &= 3a + b + g(k_2) \\ c_2 &= 3a^2 + 3a(b + g(k_2)) + (b + \gamma)g(k_2) \\ c_3 &= a^3 + 3a^2(b + g(k_2)) + 3a(b + \gamma)g(k_2) \\ c_4 &= a^3(b + g(k_2)) + 3a^2(b + \gamma)g(k_2) \\ c_5 &= a^3(b + bk_2 + \gamma)g(k_2), \end{aligned}$$

$$\text{and } g(k_2) = \frac{b(R'_0 - 1)(b + \gamma)}{b + bk_2 + \gamma}.$$

This determinant is employed to some advantage in the following simulations.

4 Numerical results

Our strategy in the simulations is to hold most parameters constant throughout the series of cases as we vary the mean delay duration, n/a , and the strength of term-time forcing as measured by $m = \lambda_2/\lambda_1$.

We fix the following parameters in all of the subsequent exercises: The Spring school term starts on day 3 and ends on day 153, and the Fall term starts on day 244 and ends on day 354. Thus, $w_1 = 105/365$ and $w_2 = 260/365$. The birth rate, b , is $1/25,000$, making the mean lifespan about 68.5 years. The recovery rate, γ , is $7/100$, so on average one is infected for about 14 days. V_m , the ceiling on the vaccination fraction, is .95. The population is 1×10^6 . Parameter k_1 , which gives the fraction who get vaccinated regardless of the past values for the disease, is $1/5$. Another “constant” is that initial conditions are always $(S(0), I(0), Y_0(0), \dots, Y_{n-1}(0)) = (60,000, 10, 10, \dots, 10)$. For ease in future discussion, we collect these assumptions in (A3).

$$\begin{aligned} w_1 &= 105/365, w_2 = 260/365, b = 1/25,000, \gamma = 7/100, \\ V_m &= .95, N = 1m, k_1 = 1/5, \text{ and} \\ R_0(\lambda_w) &> 1. \text{ Initial conditions are} \\ (S(0), I(0), Y_0(0), \dots, Y_{n-1}(0)) &= (60,000, 10, 10, \dots, 10). \end{aligned} \quad (\text{A3})$$

Other parameters are set for various situations and used for a sequence of exercises. For example, parameter k_2 , which is a metric for the strength of the delay effect, is usually set to 1800, except that we set it to zero when we look at the effect of turning delay off in order to isolate term-time forcing strength. The parameter n of the Erlang function is usually 3, though we give some examples of $n = 64$ and $n = 1$. Once these parameters are set, we consider variations in mean delay, n/a , and term-time forcing strength, $m = \lambda_2/\lambda_1$.

Our plan is to look first at a model with term-time forcing but no delay. We then look at delay without term-time forcing, and finally, we examine a combined system with both term-time forcing and delay. We are particularly curious about the sizes of m and n/a required to induce chaos. We compare the required sizes of these terms in System (2) when both delay and term-time forcing exist, when only delay exists, and when only term-time forcing exists. All simulations were run under Mathematica version number 10.3.1.0.

4.1 Term-time forcing, but no delay

We now consider a case where term-time forcing is included, but delay is turned off in the hybrid System (2). A *SIR* or *SEIR* system with term-time forcing like this has been studied by others, though not with vaccination in the model [3, 4, 13–15]. There are several options available for removing, or nearly removing, delay: (i) Since mean delay

is given by n/a , delay will approach zero as parameter a becomes large. Thus, we would “almost” eliminate delay by employing large a terms. In the hope of having a more complete break with delay, we do not use this option. (ii) We could retain the notion of prevalence demand while removing delay by linking the fraction vaccinating at time t , $V(t)$, to contemporaneous prevalence, $I(t)$. As a result, we would re-write System (1) using $\min[k_1 + k_2 I(t)/N, V_m]$ rather than $\min[k_1 + k_2 \frac{1}{N} \int_0^\infty I(t - \tau)G(\tau)d\tau, V_m]$ for the $V(t)$ component. This was the prevalence demand approach pioneered by Geoffard and Philipson [33]. The idea of prevalence demand has shed a lot of light on the difficulty of eradicating disease in that as prevalence approaches zero, the demand for vaccination diminishes (or vanishes, if $k_1 = 0$) in this construct. Nevertheless, we prefer not to use this form, feeling uncomfortable with the circularity of the idea that those making the decision to vaccinate predicate their choice on current prevalence, while current prevalence itself depends upon their choices. This model is, however, quite tractable, and can be shown to have the same R_0 values and stability conditions (though not the same paths) as we find when employing our preferred option, which follows. (iii) We choose to turn delay off by setting the endogenous response variable, k_2 , to zero. (Setting $n = 0$ would have an identical effect.) In this case the fraction vaccinating is given simply by $V(t) = k_1$. Setting $k_2 = 0$, like our previously discussed options, effectively collapses System (2) to two dimensions, since the synthetic variables Y_0, Y_1, \dots, Y_{n-1} no longer play a role. In this special case, we have

$$\begin{aligned} \frac{dS(t)}{dt} &= bN - bNk_1 - f(t)\frac{S(t)I(t)}{N} - bS(t) \\ \frac{dI(t)}{dt} &= f(t)\frac{S(t)I(t)}{N} - \gamma I(t) - bI(t). \end{aligned} \tag{System 3}$$

The equilibria for System (3) are the same as those discussed above under System (2), but stability of the pure λ_i sub-systems is much easier to investigate. The Jacobian of the pure λ_i sub-system evaluated under System (3) at (S, I) is now given by

$$J_{sys3} = \begin{pmatrix} -b - \frac{\lambda_i I}{N} & -\frac{\lambda_i S}{N} \\ \frac{\lambda_i I}{N} & \frac{\lambda_i S}{N} - b - \gamma \end{pmatrix}.$$

If we evaluate the Jacobians at $(S, I) = E_0$ and $(S, I) = E_1$, then use $R'_0(\lambda_i) = \frac{\lambda_i(1-k_1)}{b+\gamma}$, we can write the traces and determinants of J_{sys3} at the two equilibria as follows:

$$\begin{aligned} \text{at } E_0: \text{tr}(J_{sys3}) &= -b + (b + \gamma)(R'_0(\lambda_i) - 1) \text{ and } \det(J_{sys3}) = -b(b + \gamma) \\ &\quad (R'_0(\lambda_i) - 1) \\ \text{at } E_1: \text{tr}(J_{sys3}) &= -bR'_0(\lambda_i) \text{ and } \det(J_{sys3}) = -b(b + \gamma)(1 - R'_0(\lambda_i)). \end{aligned}$$

Recall that both sub-systems have the same disease-free equilibrium and that a positive endemic equilibrium only exists for a λ_i sub-system if $R'_0(\lambda_i) > 1$. It follows from application of Routh-Hurwitz to J_{sys3} that if $R'_0(\lambda_i) < 1$ for the pure λ_i sub-system, the disease-free phantom equilibrium, E_0 , will be attracting the path of the hybrid system when sub-system λ_i is in force. Similarly, if $R'_0(\lambda_i) > 1$ for the pure λ_i sub-system,

the endemic phantom equilibrium, E_1 , will be attracting the path of the hybrid system when sub-system λ_i is operative.

The two pure λ_i sub-systems of System (3) can be configured in two ways: (i) If $m > m_c$, then $R'_0(\lambda_1) < 1$. In this case, the pure λ_1 sub-system, when it is active, will be attracted to E_0 . And a positive $E_1(\lambda_1)$ will not exist. As for the pure λ_2 sub-system, (A3) implies that $R'_0(\lambda_2) > 1$, so paths will be attracted to a positive $E_1(\lambda_2)$ when that sub-system is operative. $R'_0(\lambda_2) > 1$ also implies that E_0 is unstable for the pure λ_2 sub-system. (ii) If $m < m_c$, then $R'_0(\lambda_1) > 1$, and a positive $E_1(\lambda_1)$ exists. This is locally asymptotically stable by Routh-Hurwitz. And E_0 is unstable in this case. Again, the pure λ_2 sub-system will be attracted to $E_1(\lambda_2)$ when it is switched “on.” In either case, as the positive semi-path of the hybrid system moves through time and the operative sub-systems switch, it will be attracted alternately by two different phantom “equilibrium” points.

In addition to the parameters in (A3), we assume for this section:

$$R_0(\lambda_w) = 24 \quad \text{and} \quad R'_0(\lambda_w) = 19.2. \quad (\text{A4})$$

This assumption is weakened when delay is included in the following two sections. Assumption (A3) fixes $m_c = 26.55$. Most pure temporal forcing models that find chaos use large values for R_0 . (Katriel et al. [12] use 40; Olinky et al. [16] use 24) Most studies of this sort also find chaos or irregular dynamics only when the strength of forcing (m in the present paper) is high. The simulation in this section can be regarded as a benchmark for the following sections of the paper, where we find that irregular dynamics can occur with much lower values than needed here for R_0 and forcing strength.

If $m = 1$, there is no term-time forcing, and the hybrid under the above parameters converges to a single E_1 -type endemic equilibrium. To include term-time forcing we consider cases where $m > 1$.

We begin with the modest case of $m = 1.1$, *i.e.*, when school is in session, the transmission rate, λ_2 , is 10% higher than it is during school breaks, when λ_1 is relevant. Under our assumption that $R_0(\lambda_w) = 24$, we get $(\lambda_1, \lambda_2) = (1.57, 1.73)$, implying $R_0(\lambda_1) = 22.40$ and $R_0(\lambda_2) = 24.64$, and giving $R'_0(\lambda_1) = 17.92$ and $R'_0(\lambda_2) = 19.72$. Thus, the disease-free equilibrium, which always takes the same value for both sub-systems, is unstable. The pure sub-system endemic equilibria are given by $E_1(\lambda_1) = (44634.7, 431.4)$ and $E_1(\lambda_2) = (40577, 433.7)$. Given our results on $J_{\text{sys}3}$ above, we find both pure λ_i sub-systems are stable.

The long term result is an orbit with a 1-year period, which is shown in Fig. 2. This periodic orbit is attractive, given the initial conditions shown in assumption (A3). Notice in the figure that when the summer and Christmas breaks begin, the prior upward movement in prevalence immediately changes to a decline.

We can build a tool to help us see this convergence in both the 2-D case here and more complicated settings soon to follow. Define $\psi(t; \psi(0))$ to be the solution path of System (2) from initial conditions $\psi(0) = (S(0), I(0), Y_0(0), \dots, Y_{n-1}(0))$. (In the present case, $\psi(0) = (S(0), I(0))$). If $\psi(0)$ is a point on a periodic orbit of p -year duration, then $\psi(t; \psi(0)) = \psi(t + 365p; \psi(0))$, and p is the smallest natural number satisfying this condition.

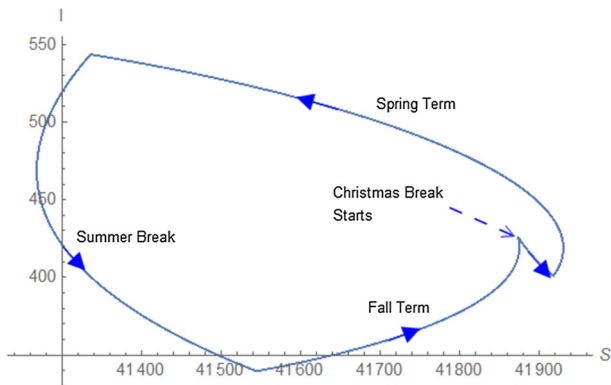


Fig. 2 One year cycle with $m = 1.1$. Plot runs over 200,000 days, beginning at $t = 3.8$ m days (in year 10411). Assumptions (A3) and (A4) apply, and $k_2 = 0$. Parameters n and a are not relevant

It is not hard to show:

Theorem 4 *If a periodic orbit exists, its period will be p years, with p a natural number*

Proof Let Γ be a generic periodic orbit in (S, I) space as shown in Fig. 3. (The graph is a heuristic sketch. Paths actually bend sharply at the “dots.”) Let $\psi(t_0)$ be a point on this orbit. Without loss of generality, we set $\psi(t_0)$ at the first day of the Spring term (day T_{Sb}) in a reference year we call y_0 . On the outside of the cycle, this point is labeled T_{Sb, y_0} and on the inside of the orbit by $\psi(t_0)$. Time advances counterclockwise around the orbit, and as it does, $\psi(t)$ passes dots marking the beginnings and ends of the school term over successive years. Starting at T_{Sb, y_0} we move along the path passing “signposts” for $T_{Se, y_0}, T_{Fb, y_0}, T_{Fe, y_0}, T_{Sb, y_1}, \dots$. By construction, T_{Fe} is always the last signpost before T_{Sb} . Hence, the incoming path to T_{Sb, y_0} which closes the cycle, must be coming from the T_{Fe} point furthest around the cycle downstream of T_{Sb, y_0} . Since we are assuming there is a periodic orbit, the path from T_{Fe, y_p} under the pure λ_1 sub-system must terminate at $T_{Sb, y_0} = T_{Sb, y_p}$, with $p \in \{1, 2, \dots\}$ being the natural number of years to complete one orbit. \square

Now suppose $\psi(0)$ is not a point on a periodic orbit, and consider the Euclidean distance between $\psi(t; \psi(0))$ and $\psi(t + 365p; \psi(0))$ for some particular value for p . Write this distance as the function $dis(\psi(t; \psi(0)), \psi(t + 365p; \psi(0)))$. We know under the present example, that $\psi(t; \psi(0))$ cannot converge to an equilibrium point as $t \rightarrow \infty$, since E_0 is unstable and the endemic equilibria are phantoms. If, as $t \rightarrow \infty$, $dis(\cdot) \rightarrow 0$ for a given p , then $\psi(t; \psi(0))$ is approaching a periodic orbit with period p years. Working numerically, this convergence is not hard to examine, and it is useful both for finding the period and for “seeing” the convergence in a high dimensional system. This distance function is depicted in Fig. 4, for the case of $m = 1.1$.

As we increase m beyond 1.1, we initially see annual cycles of the same general shape increasing in amplitude until $m \approx 1.8$. A sample of these is seen in Fig. 5.

When $m = 1.9$, the system has a 2-year cycle. The 2-year cycles are then observed until $m \approx 8$, when 4-year cycles appear. The 4-year cycles last until $m \approx 12$. Between

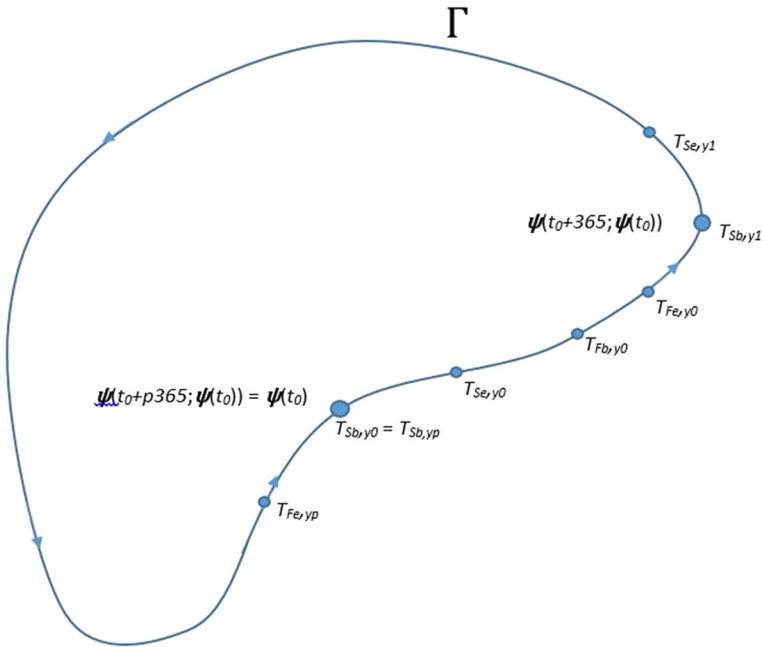


Fig. 3 A heuristic to support the argument that a closed orbit has a period which is an integer multiple of 365 days

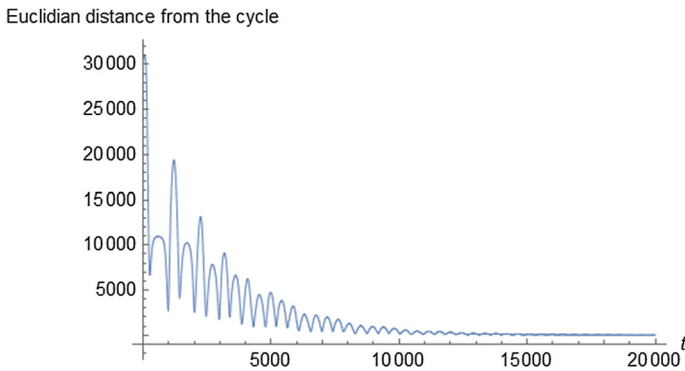


Fig. 4 Convergence to a 1-year cycle with $m = 1.1$. This shows the Euclidian distance between $\psi(t)$ and $\psi(t + 365p)$, (i.e., $dis(\psi(t), \psi(t + 365p))$), going to zero over time when $p = 1$. Parameters same as in Fig. 2

$m = 14$ and $m = 15$, we have 8-year cycles. But simple period doubling toward chaos does not happen from then on. An 11-year cycle occurs at $m = 16$. The cycle at $m = 16$ is shown in Fig. 6, using $\text{Log}(I)$ and S . Each dot in the figure marks the 153rd day of the year, i.e., the end of the Spring term. Notice that there are long periods of time when I is very close to zero (below 10^{-5}), and there are four substantial outbreaks in an 11 year period. Notice further that the path of the hybrid intersects itself several

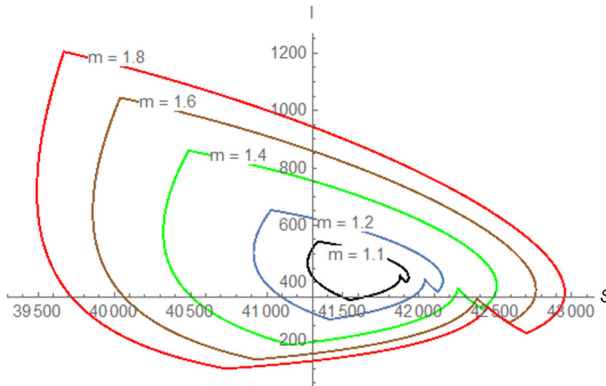


Fig. 5 This shows growth in amplitude of annual cycles as m increases from 1.1 to 18. Parameters same as in Fig. 2

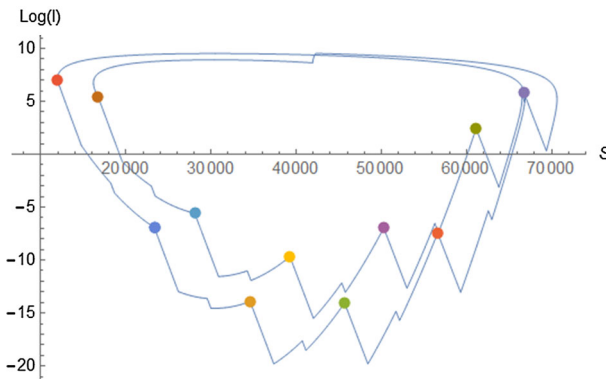


Fig. 6 An 11 year cycle running from $t = 3,651,098$ to $t = 3,655,113$, with $m = 16$. Dots mark the end of the spring school term each year. Other parameters same as in Fig. 2

times during the periodic orbit, even though the path is continuous and 2-dimensional. Neither of the two pure sub-systems will cross themselves, but one sub-system path can cross the path of the other sub-system, e.g., a “school-was-is-in” path can cross a “school-was-is-out” path.

Chaos arrives at $m \approx 17$. The time series of $I(t)$ over 70 years is shown in Fig. 7. Note the uneven interval spacings and magnitudes of outbreaks. Some of the relevant values at $m = 17$ are: $(\lambda_1, \lambda_2) = (0.14, 2.31)$; $(R_0(\lambda_1), R_0(\lambda_2)) = (1.94, 32.91)$; $(R'_0(\lambda_1), R'_0(\lambda_2)) = (1.55, 26.33)$; $E_1(\lambda_1) = (516553, 161.88)$; and $E_1(\lambda_2) = (30385.4, 439.529)$. It follows (using $\text{tr}(J_{\text{sys}3})$ and $\det(J_{\text{sys}3})$ conditions) that both pure λ_i sub-systems have positive and stable phantom endemic equilibria. Nevertheless, the hybrid formed from the two sub-systems is chaotic. See Branicky [31].

Figure 8 shows a close-up of two very different outbreaks that are highlighted in the box in Fig. 7. The dots (marked A to G) are placed at the start of each spring term. Figure 9 shows S and $\text{Log}(I)$ for the same time interval. The two graphs should be examined together. The letters in both figures identify the same points in (t, S, I) -

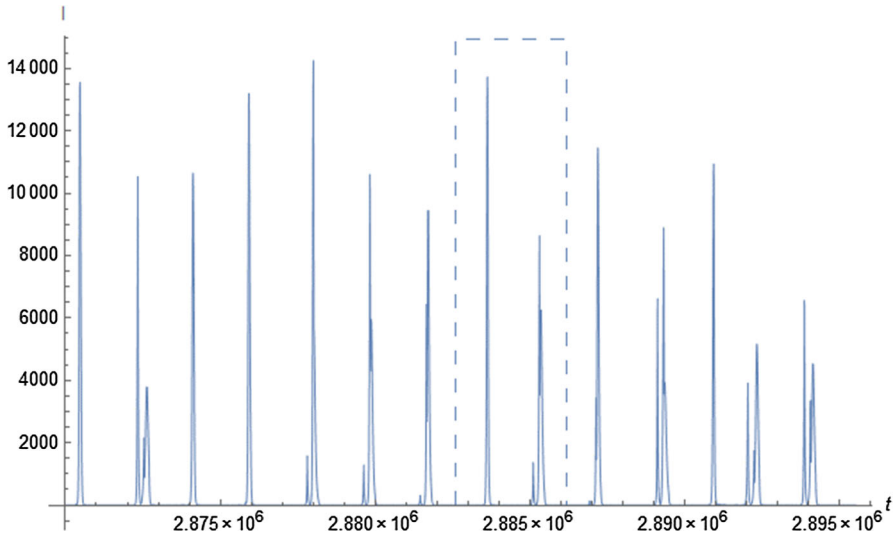


Fig. 7 Term-time forcing but no delay. Time runs for 70 years, from $t = 2,870,000$ to $t = 2,895,550$ days. Parameter $m = 17$. Other parameters same as in Fig. 2. The boxed area is discussed in the text and following two graphics

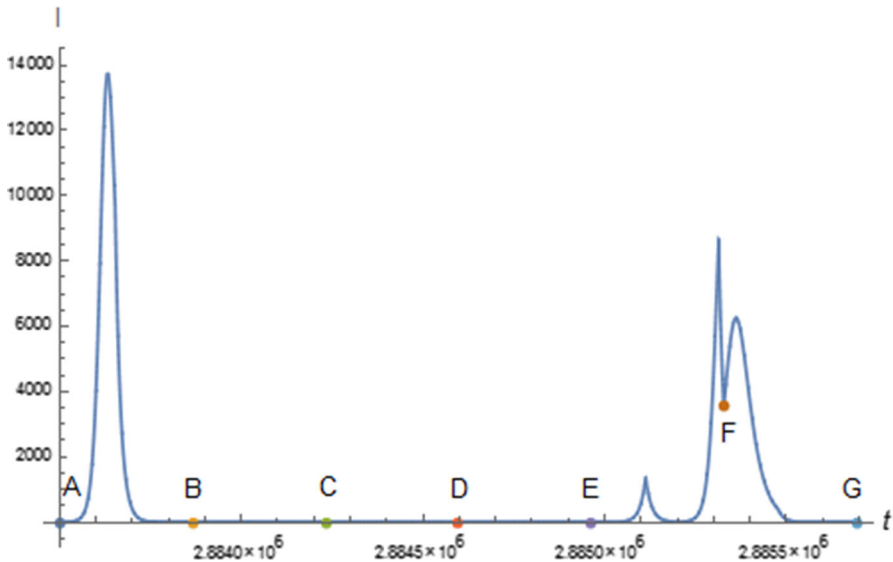


Fig. 8 Close-up of the boxed area in Fig. 7

space. Note that for long periods of time prevalence is miniscule. The high amplitude outbreak on the left (beginning at point A) peaks prior to the end of the spring term, and “burns out” many susceptibles prior to the start of the Summer break at point 1 in Fig. 9. Prevalence then falls to very low values during the succeeding fall term and Christmas break. Disease prevalence in near zero for the 3 years running from B to

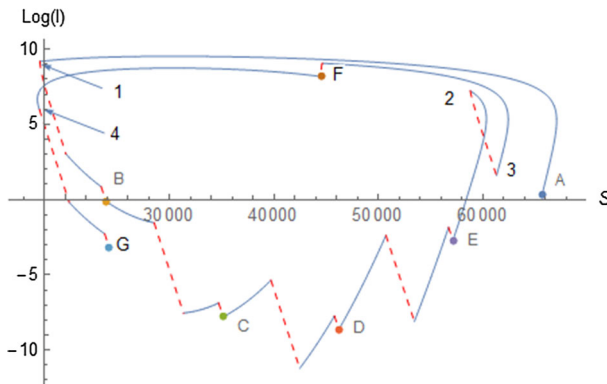


Fig. 9 Alternative view of the boxed area in Fig. 7 using Log(I) and S. Solid lines indicate school is in, and dotted lines are drawn when school is out

E. Another outbreak begins at E, which is 4 years after A. Notice from Fig. 9 that both I and S are lower at point E than point A. This gives a weaker initial outbreak, which ends at the start of summer vacation (point 2), and then takes off again in the fall (point 3). Following the Christmas break (ending at F), prevalence initially rises slightly, while the susceptible class falls dramatically. This causes prevalence to begin falling in the spring term. Point 4 marks the beginning of the summer break, and prevalence again falls to very low levels for the next few years.

Three comments: (i) The low amplitude, multiple closely-spaced peaks that are seen in the sim between E and G, are also observed in the classic childhood disease data. See Fig. 10 below, which shows monthly measles data for New York. Note the timing of the double peaks starting in 1943. (ii) Note from Fig. 7 that these twin peaks can be quite common in the model. (iii) Interestingly, if one measures the number of cases in the two years between points A and C (the single large outbreak case) by forming $\gamma \int_A^C I(t)dt$, the result is 52926, while integrating between E and G (the “twin peak” case) gives $\gamma \int_E^G I(t)dt = 55059$, a roughly 4% difference. Katriel and Stone [12], who modeled attack rates using sinusoidal forcing, showed something related to this, finding that attack rates over long time spans were very close whether or not seasonal forcing is included.

A bifurcation summary diagram is shown in Fig. 11. The diagram is generated as follows: Simulations are run from $t = 0$ to $t = 4 \times 10^6$ for a multitude of values of m , from $m = 1$ to $m = 50$. Values of I are then taken over a 400 year interval between $t = 3,651,248$ and $3,797,248$, and a dot is generated on the last day of the spring term for each year. If the system has a stable p -year cycle, p different dots appear. For example, if System (2) has a stable annual cycle, the algorithm will generate 400 dots, but they will all be the same. This would happen if the case shown in Fig. 2 cycled 400 times. When p is large, there may be a stable long-period cycle, or there may be chaos.

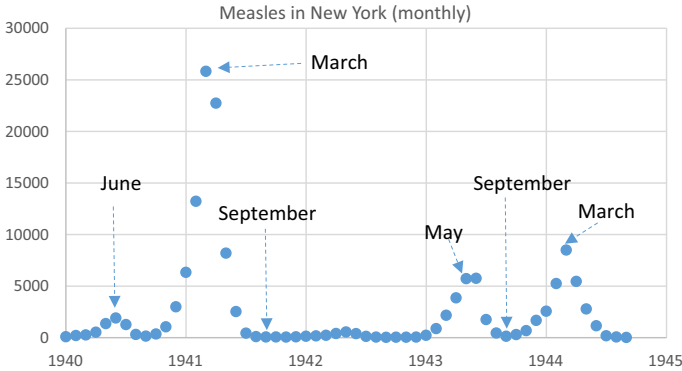


Fig. 10 Monthly data on measles in New York. *Source:* <http://ms.mcmaster.ca/~bolker/measdata/nycmeas.dat>

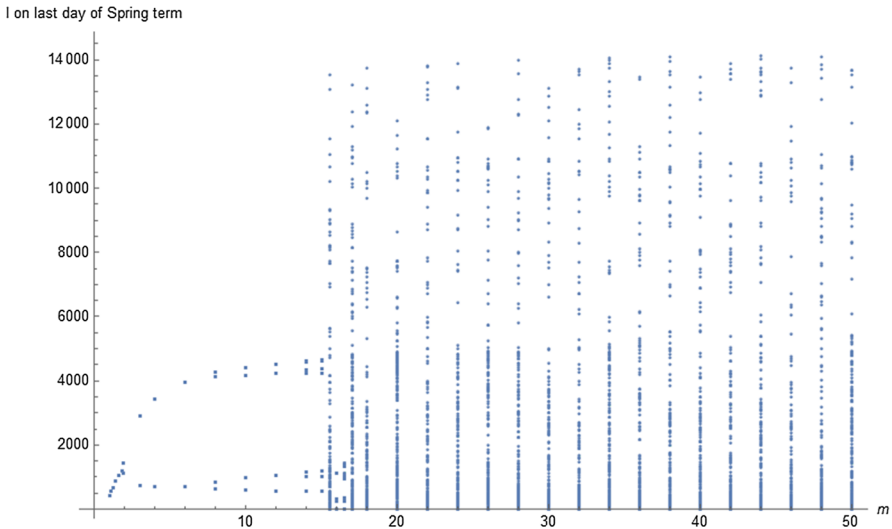


Fig. 11 Bifurcation diagram for pure term-time forcing under assumptions of Fig. 2

As m rises past 17, we continue to see chaos through at least $m = 50$. We are not aware of empirical studies that establish reasonable bounds for m in a *SIR* structure with vaccination, but we note that London and Yorke’s [34] measles study had ratios of high to low contact rates for measles, chickenpox, and mumps on the order of 1.7. Fine and Clarkson [35] found the ratios of contact rates for measles in the range of 2–3. See Keeling and Rohani [36] for further discussion. This section has a slight twist (inclusion of vaccination) on established results for term-time forcing models. Our admittedly arbitrary justification for not going past $m = 50$ is the following: When m increases $S_1(\lambda_1)$ rises and $I_1(\lambda_1)$ falls, with $I_1(\lambda_1)$ reaching 0, when $\lambda_1 = \frac{b+\gamma}{1-k_1} = .08755$ under our present parameters. This in turn requires $m = 26.55$, which eliminates a positive $E_1(\lambda_1)$ and gives stability to $E_0(\lambda_1)$. This, in turn, would mean the disease would

ultimately disappear if school were never in session. Though we can't rule this out, we feel that roughly doubling $m = 26.55$ to $m = 50$, will cover our area of interest.

We have examined this “no-delay” case in order to provide a benchmark for results we get later in this section, where we have both term-time forcing and delay in the response of vaccination demand to past prevalence. The key point so far from this section is that chaos can result from term-time forcing when both $R_0(\lambda_w)$ and m are “large” (24 and 18, respectively).

4.2 Delay, but no term-time forcing

In this section we look at two closely related *SIR* models with distributed delay between disease outbreaks and vaccination response, *but without term-time forcing*. We retain all assumptions in (A3), except that we now set $k_2 = 1800$ and reduce $R_0(\lambda_w)$ to 16. For ease of reference, we write this as

$$k_2 = 1800, R_0(\lambda_w) = 16. \quad (\text{A5})$$

We retain (A5) through the remainder of the paper. The idea in this section is to check the effects of delay in the absence of term-time forcing. This section provides a second benchmark prior to our results in the next section, where delay and term-time forcing are modeled together.

The first model of this section sets the degree of the Erlang function at $n = 3$, and the second uses $n = 64$. Recall that n (along with parameter a) gives the shape of Erlang function, which assigns weights to all past values of prevalence, and which then (along with parameters k_1 and k_2) determines the current fraction demanding vaccination. The mean delay duration of the Erlang distribution is given by n/a , and the standard deviation of the distribution is \sqrt{n}/a . Thus, the ratio of the standard deviation to the mean delay is $1/\sqrt{n}$, and the dispersion about a given mean falls as n increases. For example, if we are interested in a mean delay of 180 days, then if our model sets n at 3, the standard deviation around 180 will be 103.9 days, but if we model the same mean delay with $n = 64$, the standard deviation would be 22.5 days.

4.2.1 $n = 3$.

We start with the $n = 3$ case, assuming there is no term-time forcing, (i.e., $\lambda_1 = \lambda_2 = 1.12$). Other parameters are as given in (A3) and (A5). After many simulation runs using various delay durations, we get the bifurcation diagram shown in Fig. 12. Mean delay increases to the right along the horizontal axis. The vertical axis shows: (i) I_1 as a solid line, if E_1 is stable; (ii) I_1 as a dashed line, if E_1 is unstable; and (iii) the maximum and minimum values of I (noted I_{max} and I_{min} , respectively) along a periodic orbit at various values for mean delay. For better optics, we use $\text{Log}_{10}(I)$ of all I values.

To the far left of Fig. 12, when mean delay is between 0 and about 16 days, E_1 is locally stable. Beyond a mean delay of about 1151 days, E_1 is again locally stable. The “orbit” drawn is just a sketch indicating that periodic orbits form. The transition

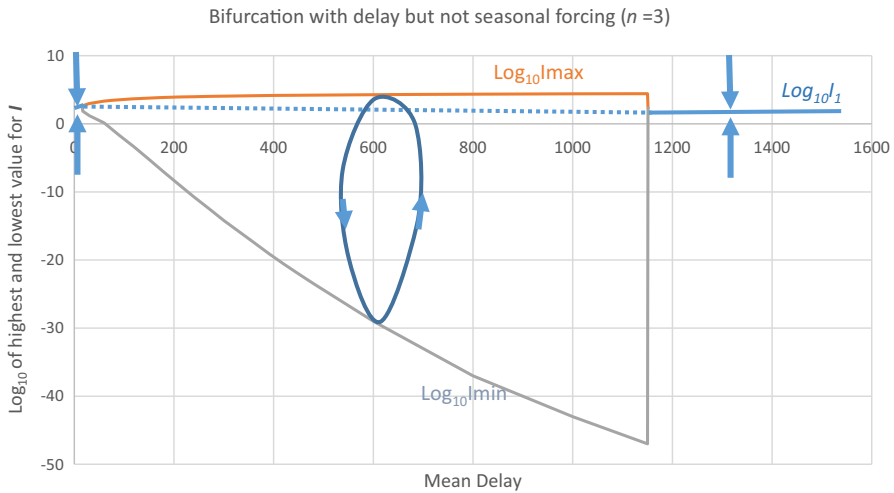


Fig. 12 Equilibrium values for $\text{Log}_{10}(I_1)$ when E_1 is stable, or the maximum and minimum of $\text{Log}_{10}(I_1)$ when E_1 is unstable, shown as a function of the mean delay interval. There is no term-time forcing. Parameters from (A3) and (A5)

points, where mean delays are about 16 and about 1151, are found by numerically solving $\det(H_4(a)) = 0$ for any real and positive roots. In this case, there are two real positive a values giving $\det(H_4(a)) = 0$; these define the mean delay times where stability switches occur. We call them a_L and a_H , for lower and higher, respectively. $\det(H_4(a)) > 0$ and E_1 is stable for $a < a_L$ and for $a > a_H$. Otherwise $\det(H_4(a)) < 0$ and E_1 is unstable. The expression n/a then gives the associated mean delay, where $n = 3$ in this case. Notice in Fig. 12 that as mean delay increases, I_{max} grows. This is to be expected, since delayed vaccination response allows the disease to proliferate. It is also the case that the interval between peak outbreaks rises as mean delay increases. The periods are shown as a function of mean delay in Fig. 13. As delay increases, the intensity of the outbreaks rise, while their frequency falls. This raises the question about the long term impact of the disease as the mean delay rises. We check this looking at $\gamma \int_{t_i}^{t_j} I(t) dt$ over a long interval, where $t_i = 3 \times 10^6$ and $t_j = 4 \times 10^6$ days. This gives the total number of cases (divided by 10^7 in the figure) during a million-day span. These results are also displayed in Fig. 13. (Data in both Figs. 12 and 13 are discrete, but presented continuously to enhance optics.)

Figure 14 shows a typical sim result projected to (S, I) space, where mean delay is 90 days. One sees a path spiraling out from an initial point near the unstable E_1 and moving toward an orbit which is shown running from 3.9×10^6 to 4.0×10^6 days. Notice that we do not get irregular dynamics. Depending upon the value of mean delay, we see either convergence to E_1 or to various sized cycles. After doing extensive simulations with plausible parameter sets, we have not been able to generate irregular dynamics with Erlang parameter $n = 3$ and no term-time forcing. Of course,

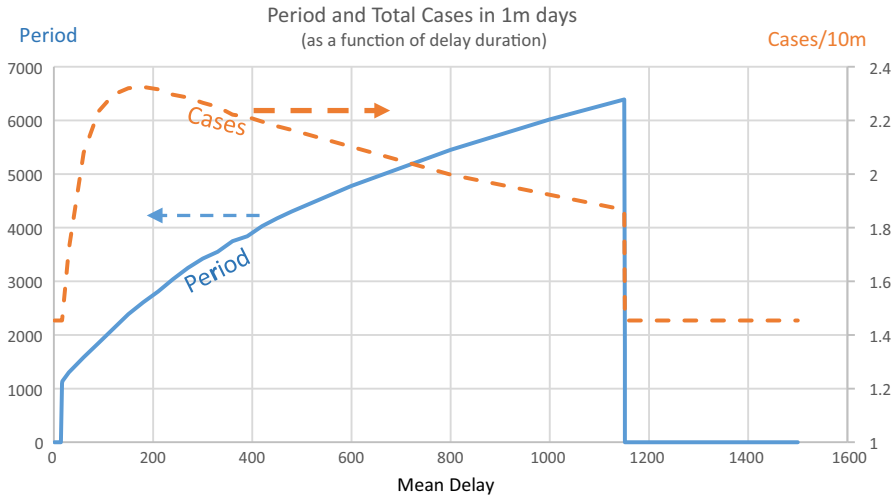


Fig. 13 This shows the period of oscillations and the total number of cases (divided by 10^7) over a million day interval as functions of mean delay. Parameters from (A3) and (A5)

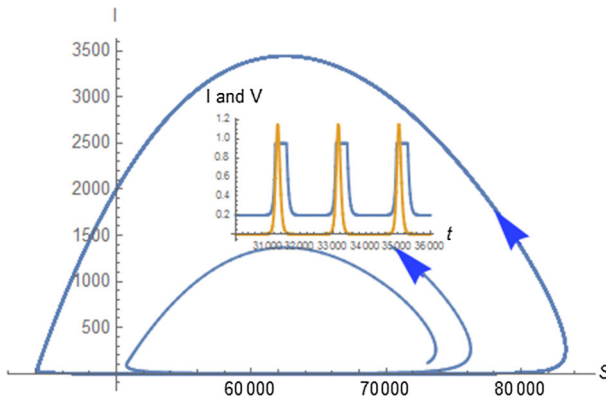


Fig. 14 Mean delay is 90 days and $n = 3$. A path is spiraling is out from an unstable E_1 toward a periodic orbit. The inset shows prevalence levels/3000 for scaling (brown) and delayed vaccination response (blue)

a finite number of trials does not establish impossibility. We will now see that irregular dynamics follows easily when higher levels of n are used.

4.2.2 $n = 64$.

While retaining for the moment our temporary assumption of no term-time forcing, we leave the parameters above intact, except that we increase n to 64. This allows us to tighten the standard deviation around the mean delay. As expected, this system yields a locally stable E_1 for low values (about two weeks) of mean delay. With delay durations above (roughly) two weeks, E_1 is unstable and approaches a periodic orbit much like that shown in Fig. 14. These cycles are at first single peaked, and on a period

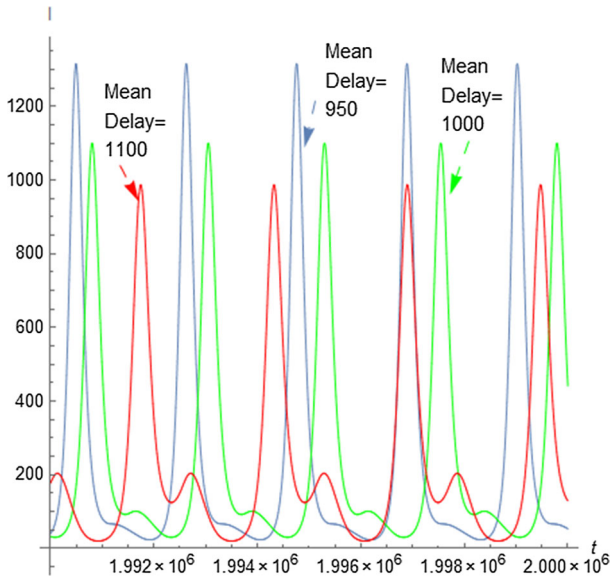


Fig. 15 Time series for various delay durations, with $n = 64$, no term-time forcing, and parameters in (A3) and (A5)

of a little more than 2000 days. But as mean delay rises past about 950 days, the post outbreak interval begins to show, at first, a wiggle and then a minor secondary peak. This secondary peak grows in size without substantially increasing the duration of the periodic orbit—it goes from about 2100 days at mean delay of 950 to about 2560 days with mean delay 1100 days. See Fig. 15.

By mean duration delay of 1110 days, the period has roughly doubled to about 5200 days with 4 prevalence peaks appearing in the periodic orbit. This period doubling happens again as the mean delay hits about 1144 days. There are now 8 distinct peaks in a roughly 10,700 day periodic orbit. A cascade has begun, and by mean delay 1150 days, there are 16 prevalence peaks on a periodic orbit 21,712 days long. This is roughly the same length as the mean lifespan. See Fig. 16, where we show prevalence, $I(t)$, and the fraction vaccinating, $V(t)$, over 25,000 days, ending at day 2×10^6 . Here the reader can see the fraction vaccinating reaching its ceiling value of 0.95 following large outbreaks.

Longer delays produce chaotic-looking outcomes, one of which we illustrate in Fig. 17. Here mean delay is 1160 days. The variable Y_{64} is one of the synthetic variables used with the linear chain trick.

This and the previous section were meant to establish two benchmarks. In Sect. 4.1 we showed that, *in the absence of delay*, term-time forcing could cause irregular dynamics if the forcing is “strong,” i.e., a large difference between disease transmission parameters when school is out versus in. The main results of the numerical exercise in present sub-section are: (i) *When term-time forcing is not present*, the SIR model with vaccination responding to past prevalence under Erlang distributed delay with $n = 3$ appears to give orderly dynamics for all values of mean delay. (ii) Chaotic dynamics

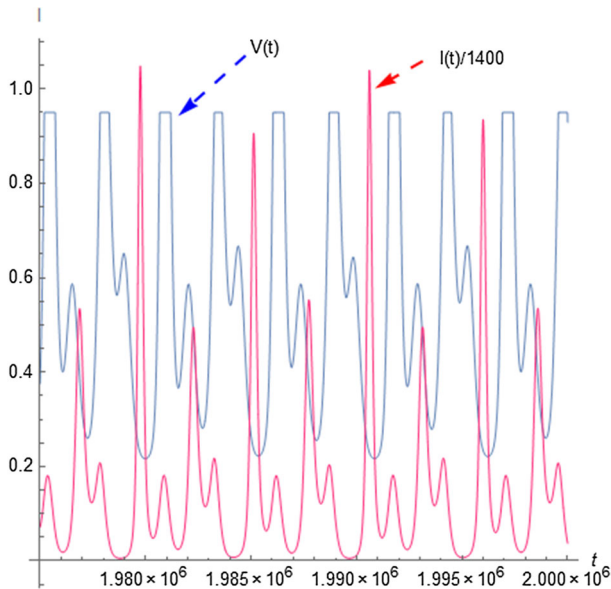


Fig. 16 Mean delay is 1150, with $n = 64$, no term-time forcing, and parameters in (A3) and (A5). A cycle of duration 21,712 days having 16 different prevalence peaks occurs

are found to be possible *without* term-time forcing when n is large and mean delay is “long.” In the next section we investigate a model with both term-time forcing and delay.

4.3 Both term-time forcing and delay

Following in the path of d’Onofrio, Manfredi, and Salinelli [24,27], who explored the combination of sinusoidal forcing of contact rates and prevalence induced vaccination choices of various forms, we now examine System (2) with both discrete school-related term-time forcing and distributed delay under a range of Erlangian parameters.

Recall from the discussion of Fig. 14 that when $\lambda_1 = \lambda_2$, (equivalently, when $m = 1$), and there is no term-time forcing, we get a simple periodic orbit when: the Erlang parameter $n = 3$, mean delay is 90 days, and both assumptions (A3) and (A5) hold. We also learned there that in order to get more exotic dynamics n needs to be larger as does the mean delay. We begin this section using the result displayed in Fig. 14 as a baseline and introducing term-time forcing by gradually increasing m , while holding $n = 3$ and mean delay equal to 90 days.

We hold all other parameters as they were, and we continue to constrain $R_0(\lambda_w)$ to 16. Thus, the weighted average of λ_2 and λ_1 is fixed.

Consider first the case where λ_2 is just 10% above λ_1 , i.e., $m = 1.1$. Recall that the two pure λ_i sub-systems might have endemic equilibria, but the full hybrid system will not. Nevertheless, the positions and stability properties of the “phantom” equilibria are of interest. In the present case, $E_1(\lambda_1) = (66952.1, 206.434)$ and $E_1(\lambda_2) =$

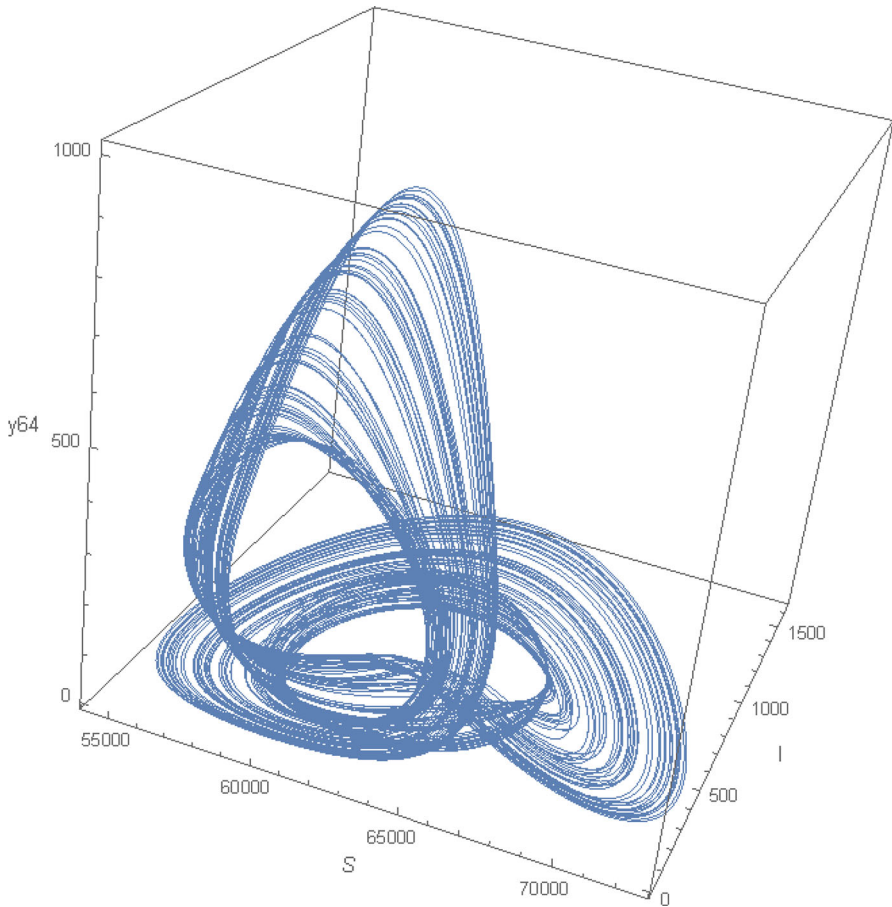


Fig. 17 Mean delay is 1160, with $n = 64$, no term-time forcing, and parameters in (A3) and (A5). Time runs from $t = 1.8 \times 10^6$ to 2×10^6

(60865.5, 208.148). In general, the two points separate as m increases beyond $m = 1$. This can be seen by noting that

$$E_1(\lambda_i) = (S_1(\lambda_i), I_1(\lambda_i)) = \left(\frac{N(b + \gamma)}{\lambda_i}, \frac{bN(-b - \gamma + \lambda_i(1 - k_1))}{(b + bk_2 + \gamma)\lambda_i} \right) \quad i = 1, 2.$$

Since $R_0(\lambda_w)$ is a convex combination of λ_1 and λ_2 , when λ_2 increases, λ_1 falls. Further, when the value of λ_2 rises, it is obvious that $S_1(\lambda_2)$ falls and $I_1(\lambda_2)$ rises. Similarly, when λ_1 falls, $S_1(\lambda_1)$ rises, and $I_1(\lambda_1)$ falls. It follows that when m increases from $m = 1$, these changes cause $E_1(\lambda_1)$ and $E_1(\lambda_2)$ to move apart.

In the present example, both the pure λ_1 and λ_2 sub-systems are locally unstable. This is verified using $\det(H4)$. The result with $m = 1.1$ is the 5-year periodic orbit shown in Fig. 18.

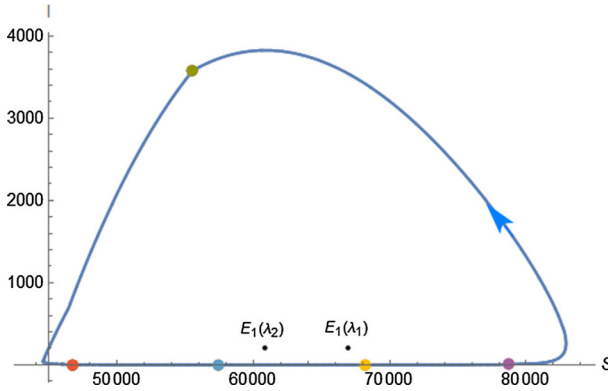


Fig. 18 Assumptions (A3) and (A5) hold. Mean delay is 90 days, $m = 1.1$, and $n = 3$. Time runs once through a 5-year periodic orbit starting at $t = 3,987,043$. Dots mark the last day of the Spring term

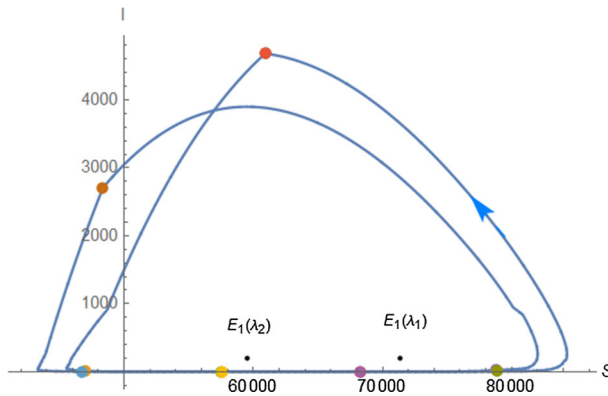


Fig. 19 Here we see period doubling beginning at about $m = 1.2$ with 90 day mean delay and $n = 3$. Other parameters are given in (A3) and (A5). Time runs for 10 years beginning at $t = 3,907,843$. Dots mark the end of each Spring term. There are 10 dots, the ones at the bottom nearly overlap

We now set λ_2 20% above λ_1 . The result is that the full hybrid system undergoes a period doubling bifurcation, as see in Fig. 19. The two phantom equilibria are $E_1(\lambda_1) = (71404.1, 205.2)$ and $E_1(\lambda_2) = (59503.4, 208.5)$. Both are unstable. The obvious kinks in the trajectory are due to the temporal forcing events, but the trajectory will also bend perceptibly when the vaccinating fraction switches between $\min[k_1 + k_2 Y_2/N, V_m] = k_1 + k_2 Y_2/N$ and the ceiling value $\min[\cdot] = V_m$, as $Y_2(t)$ moves through the state space under System (2). The path in Fig. 19 appears to cross itself, but it actually does not. The figure is really just a 2-D slice of a 5-D system.

We continue boosting the strength of the term-time forcing by increasing λ_2 modestly from 20% above λ_1 to 22% above λ_1 . (Since we are holding λ_w and $R_0(\lambda_w)$ constant, λ_1 falls slightly as λ_2 increases.) The result is shown in Fig. 20. Both phantom endemic equilibria (the two dots in the figure) are unstable. The hybrid system has undergone another period doubling bifurcation, with

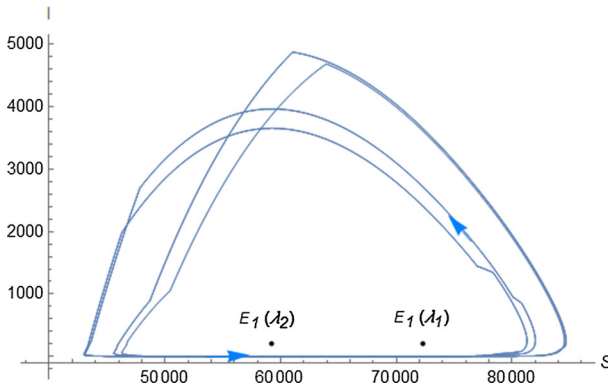


Fig. 20 Another period doubling with forcing strength now at $m = 1.22$ with 90 day mean delay and $n = 3$. Other parameters are given in (A3) and (A5). Time runs for 10 years beginning at $t = 3,911,390$

the period now 20 years long and with major outbreaks still occurring every 5 years.

With $m = 1.225$, there is another period doubling bifurcation, with a 40 year period and 5 year intervals between outbreaks. Increasing m to 1.23, the hybrid begins to look chaotic. Figure 21 shows a 3-D slice of the hybrid (including one of the synthetic variables, Y_2) with time running from $t = 2.8 \times 10^6$ to 3.0×10^6 days.

When $m = 2$, the chaos is much more evident. This is seen in the two following time series plots of $I(t)$ shown in Figs. 22 and 23. The first spans 200,000 days following $t = 3.8 \times 10^6$, and the second gives better resolution at a shorter time span.

Figure 23 gives the fine structure of the time path of I , with t running from 3,806,000 to 3,825,000 days. The period between outbreaks is irregular, and the outbreaks themselves vary greatly in the height of the major peaks and in the number and arrangement of lesser peaks. Notice that we again see a mix of large outbreaks and closely-packed, relatively low amplitude peaks, as we did in Fig. 8.

Before we look at our final example, we recap the results of the previous sections.

- (i) In Sect. 4.1 we saw that term-time-generated changes in contact rates can engender irregular cycles in the absence of vaccination demand delay when both $R_0(\lambda_w)$ and the forcing strength are high. Specifically, we found this when $R_0(\lambda_w) = 24$ and $m = 17$.
- (ii) In Sect. 4.2 we saw that when delay is employed, but term-time forcing is off, we cannot find irregular dynamics without employing high degree Erlang functions ($n = 64$ in the case examined) and long (1150 day) mean delay, though we did get this result with $R_0(\lambda_w)$ equal to a more modest 16.
- (iii) So far in Sect. 4.3, where we have combined term-time forcing and vaccination response delay, we have found chaos with relatively low levels of term-time forcing strength (m equal 2 or less) and 90 day mean delay. We have shown this with Erlang distributions with n equal to 3. But the next example shows that moderate term-time forcing ($m = 2$) coupled with reasonable mean delay (90 days) can also produce chaos in the $n = 1$ case. That is, term-time forcing substantially reduces the demands on the delay structure and

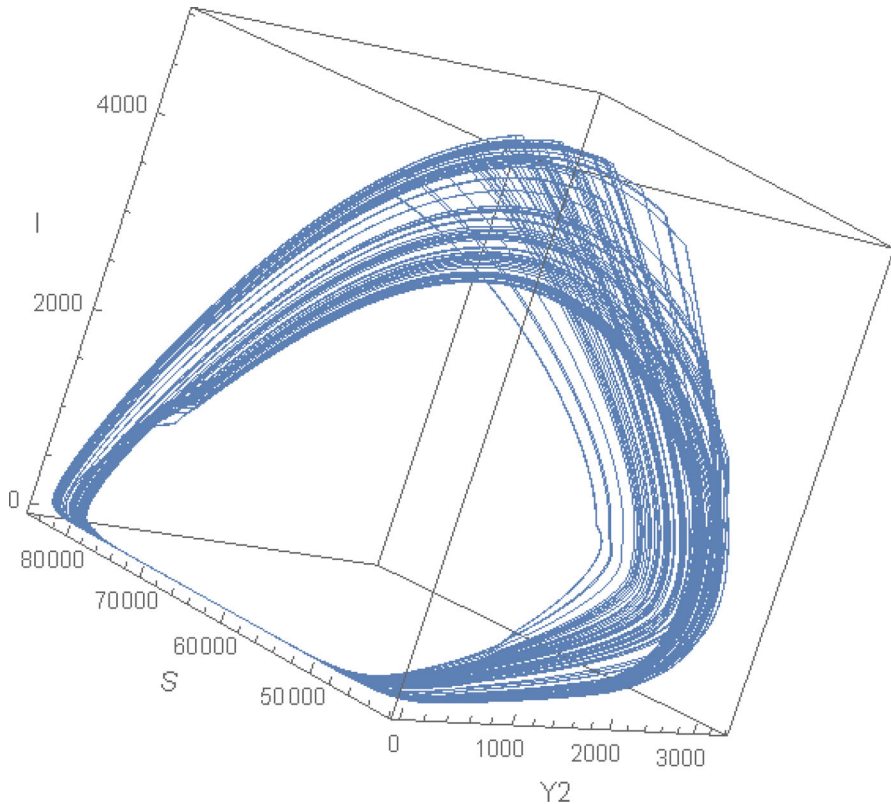


Fig. 21 Chaos starts at about $m = 1.23$ with 90 day mean delay and $n = 3$. Other parameters are given in (A3) and (A5). Time runs for 200,000 days beginning at $t = 2.8$ m

moderate delay reduces the demands on term-time forcing strength in order to obtain irregular dynamics. Hence, the word “complementarity” in the title.

In Sect. 2 we gave reasons for thinking that values for n above one are more appropriate for vaccination delay. Our reasons were that: First, today’s level of prevalence should not be used to explain today’s vaccination demand, as it does when $n = 1$. And second, a “bell-shaped” distribution seems reasonable, in that we conjecture that a few people respond quickly to an outbreak, then as the delay time rises, more people will respond, and then response trails off. But there is no denying that working with $n = 1$ is more likely to yield analytical results, thanks to the work of Buonomo et al. [19,20], d’Onofrio et al. [21,22]. And empirically the $n = 1$ case may produce good results.

With $n = 1$ and all other parameters unchanged (except that parameter a is adjusted to maintain mean delay of 90 days), we again see irregular periods and amplitudes plus a mix of large single peaked outbreaks and longer-running multi-peak events. The example is shown in Fig. 24.

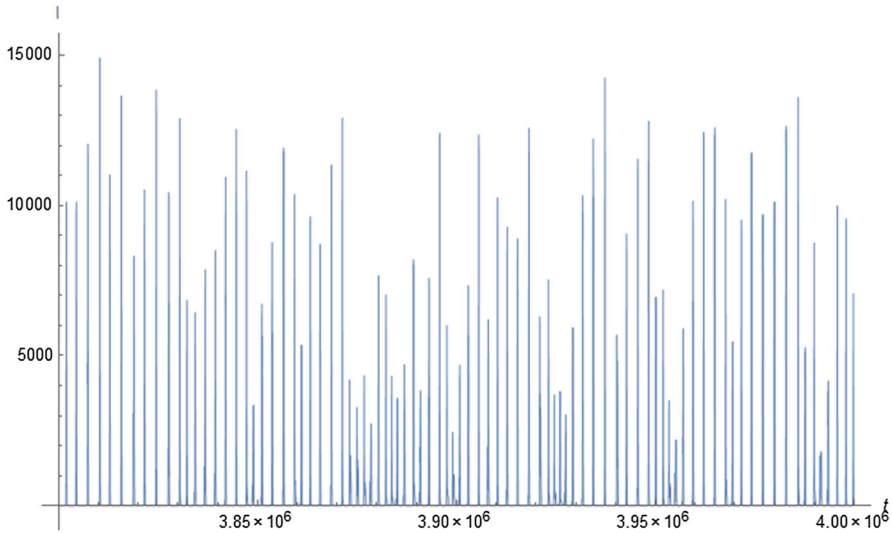


Fig. 22 Here term-time forcing strength is given by $m = 2$. There is 90 day mean delay with $n = 3$. Other parameters are given in (A3) and (A5). Time runs for 200,000 days beginning at $t = 3.8 \times 10^6$

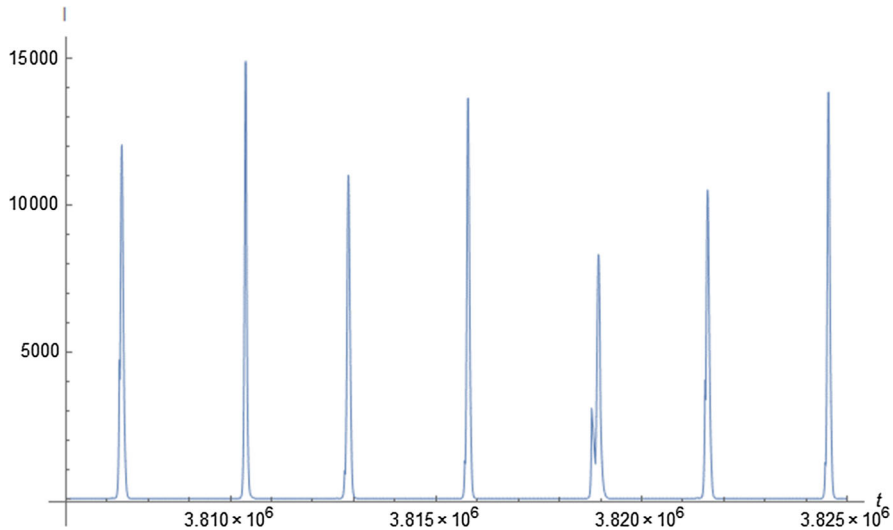


Fig. 23 Parameters same as in Fig. 22, except time interval shown is only about 50 years, starting at $t = 3,806,000$

5 Conclusion

Many researchers have made a strong case for term-time forcing. There is little doubt that the congregation of students during the school term enhances disease transmissibility. It seems undeniable, also, that individuals contemplating vaccination respond with a delay when a disease outbreak occurs. It also seems clear empirically that disease

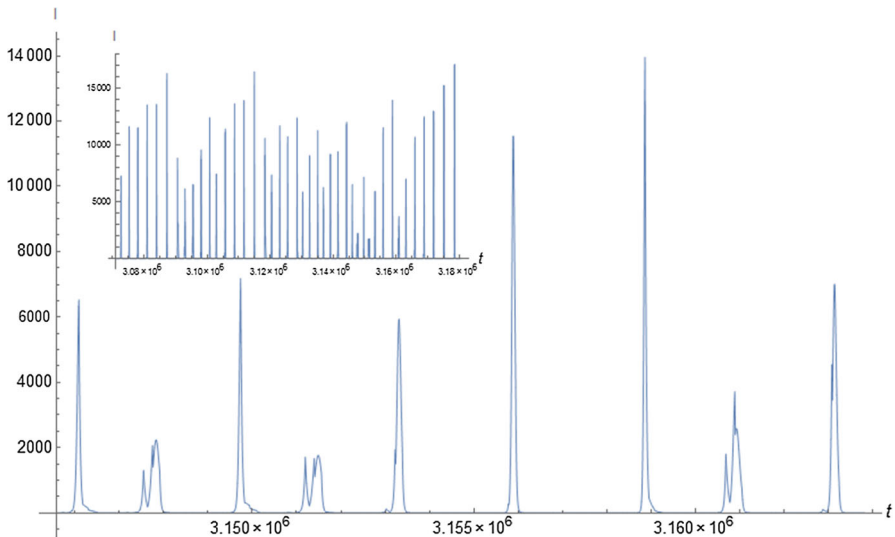


Fig. 24 Term-time forcing coupled with delay with the “weak kernel.” Here $n = 1$, $m = 2$, mean delay = 90 days, and both (A3) and (A5) hold. The main graph shows six major outbreaks over a 50 year interval starting at $t = 3,145,573$, the first day of the Spring term of reference year 8618. The inset shows a longer time span (about 300 years) surrounding the main graph

dynamics are irregular in the sense that neither convergence to an endemic equilibrium nor a simple periodic orbit is the norm. Researchers working with temporal forcing (both sinusoidal and discrete) in otherwise conventional *SIR* models have found that only “strong” forcing can bring about irregular dynamics. Similarly, delay models of many sorts seem to lead to irregular dynamics only when delay is “long” (See Buric and Todorovic [37], Canabarro et al. [38], Hao et al. [39], Jiang et al. [41], Mackey and Glass [40], and Vasegh et al. [42]). This exercise, along with [24, 27] has shown that models with *both* term-time forcing *and* vaccination delayed response to prevalence can display irregular dynamics with moderate forcing strength and reasonable mean delay durations.

Purely analytical result have been elusive in both simple term-time forcing models and simple delay models. No doubt that will change in time, but at the moment we can show numerically how the combination of forcing and delay can work with commonly used population/disease parameters. This may be helpful in statistical modelling, but that will be another story.

Acknowledgements This paper has benefited enormously from the authors’ exchanges with the editors and two anonymous referees.

References

1. Brauer, F., van den Driessche, P., Wu, J.: *Mathematical Epidemiology*. Springer, Berlin (2008)
2. Manfredi, P., D’Onofrio, A.: *Modeling the Interplay Between Human Behavior and the Spread of Infectious Diseases*. Springer, New York (2013)

3. Schenzle, D.: An age structured model of pre- and post-vaccination measles transmission. *IMA J. Math. Appl. Med. Biol.* **1**, 169–191 (1984)
4. Bolker, B., Grenfell, B.: Chaos and biological complexity in measles dynamics. *Proc. R. Soc. Lond. B Biol. Sci.* **251**, 75–81 (1993)
5. Bolker, B.: Chaos and complexity in measles models: a comparative numerical study. *IMA J. Math. Appl. Med. Biol.* **10**, 83–95 (1993)
6. Soper, H.: The interpretation of periodicity in disease prevalence. *J. R. Stat. Soc. Ser. A Stat. Soc.* **92**, 34–61 (1929)
7. Bartlett, M.: Measles periodicity and community size. *J. R. Stat. Soc. Ser. A Stat. Soc.* **120**, 48–70 (1957)
8. Bailey, N.: *The Mathematical Theory of Infectious Diseases and Its Applications*. Griffin, London (1975)
9. Aron, J., Schwartz, I.: Seasonality and period-doubling bifurcations in an epidemic model. *J. Theor. Biol.* **110**, 665–679 (1984)
10. Acedo, L., Morano, J., Santonja, F., Villanueva, R.: A deterministic model for highly contagious diseases: the case of varicella. *Physica A* **450**, 278–286 (2016)
11. Billings, L., Schwartz, I.: Exciting chaos with noise: unexpected dynamics in epidemic outbreaks. *J. Math. Biol.* **44**, 31–48 (2002)
12. Katriel, G., Stone, L.: Attack rates of seasonal epidemics. *Math. Biosci.* **235**, 56–65 (2012)
13. Earn, D., Rohani, P., Bolker, B., Grenfell, B.: A simple model for complex dynamical transitions in epidemics. *Science* **287**, 667–670 (2000)
14. Keeling, M., Rohani, P., Grenfell, B.: Seasonally forced disease dynamics explored as switching between attractors. *Physica D* **148**, 317–335 (2001)
15. Rohani, P., Keeling, M., Grenfell, B.: The interplay between determinism and stochasticity in childhood diseases. *Am. Nat.* **159**, 469–481 (2002)
16. Olinky, R., Huppert, A., Stone, L.: Seasonal dynamics and thresholds governing recurrent epidemics. *J. Math. Biol.* **56**, 827–839 (2008)
17. Diedrichs, D., Ishihara, P., Buursma, D.: The schedule effect: can recurrent peak infections be reduced without vaccines, quarantines or school closings? *Math. Biosci.* **248**, 46–53 (2013)
18. Zhao, D.: Study on the threshold of a stochastic SIR epidemic model and its extensions. *Commun. Nonlinear Sci. Numer. Simul.* **38**, 172–177 (2016)
19. Buonomo, B., d’Onofrio, A., Lacitignola, D.: Global stability of an SIR epidemic model with information dependent vaccination. *Math. Biosci.* **216**, 9–16 (2008)
20. Buonomo, B., d’Onofrio, A., Lacitignola, D.: Modelling of pseudo-rational exemption to vaccination for SEIR diseases. *J. Math. Anal. Appl.* **404**, 385–398 (2013)
21. d’Onofrio, A., Manfredi, P., Salinelli, E.: Vaccinating behaviour, information, and the dynamics of SIR vaccine preventable diseases. *Theor. Popul. Biol.* **71**, 301–317 (2007)
22. d’Onofrio, M., Manfredi, P., Poletti, P.: The interplay of public intervention and private choices in determining the outcome of vaccination programmes. *PLoS ONE* **7**(10), 1–10 (2012)
23. Greenhalgh, D., Khan, Q., Lewis, F.: Recurrent epidemic cycles in an infectious disease model with a time delay in loss of vaccine immunity. *Nonlinear Anal. Theory Methods Appl.* **63**, e779–e788 (2005)
24. d’Onofrio, A., Manfredi, P.: Information-related changes in contact patterns may trigger oscillations in the endemic prevalence of infectious diseases. *J. Theor. Biol.* **256**, 473–478 (2009)
25. Eckalbar, J., Eckalbar, W.: Dynamics of an SIR model with vaccination dependent on past prevalence with high-order distributed delay. *BioSystems* **129**, 50–65 (2015)
26. Eckalbar, J., Eckalbar, W.: Dynamics in an SIR model when vaccination demand follows prior levels of disease prevalence. *Adv. Complex Syst.* **18**, 1–27 (2015)
27. d’Onofrio, A., Manfredi, P., Salinelli, E.: Vaccinating behaviour and the dynamics of vaccine preventable infections. In: Manfredi, P., d’Onofrio, A. (eds.) *Modeling the Interplay Between Human Behavior and the Spread of Infectious Diseases*. Springer, New York (2013)
28. Ruan, S.: Delay differential equations in single species dynamics. In: Arino, O., Hbid, M., Ait, Dads, E. (eds.) *Delay Differential Equations and Applications*, pp. 477–517. Springer, Berlin (2006)
29. MacDonald, N.: *Time Lags in Biological Models*. Springer, New York (1978)
30. Smith, H.: *An Introduction to Delay Differential Equations with Applications to the Life Sciences*. Springer, New York (2011)
31. Branicky, M.: Multiple Lyapunov functions and other analysis tools for switched and hybrid systems. *IEEE Trans. Autom. Control* **43**(4), 475–482 (1998)

32. Crommelin, J., Opsteegh, J., Verhulst, F.: A mechanism for atmospheric regime behavior. *J. Atmos. Sci.* **61**, 1406–1419 (2004)
33. Geoffard, P., Philipson, T.: Disease eradication: private versus public vaccination. *Am. Econ. Rev.* **87**, 222–230 (1997)
34. London, W., Yorke, J.: Recurrent outbreaks of measles, chickenpox, and mumps, I. Seasonal variation in contact rates. *Am. J. Epidemiol.* **98**, 453–468 (1973)
35. Fine, P., Clarkson, J.: Measles in England and Wales—I: an analysis of factors underlying seasonal patterns. *Int. J. Epidemiol.* **11**, 5–14 (1982)
36. Keeling, M., Rohani, P.: *Modeling Infectious Diseases in Humans and Animals*. Princeton University Press, Princeton (2008)
37. Buric, N., Todorovic, D.: Dynamics of delay-differential equations modeling immunology of tumor growth. *Chaos Solitons Fractals* **13**, 645–655 (2002)
38. Canabarro, A., Gleria, I., Lyra, M.: Periodic solutions and chaos in a non-linear model for the delayed cellular immune response. *Physica A* **382**, 238–241 (2004)
39. Hao, L., Jiang, G., Liu, S., Ling, L.: Global dynamics of an SIRS epidemic model with saturation incidence. *BioSystems* **114**, 56–63 (2013)
40. Mackey, M., Glass, L.: Oscillation and chaos in physiological control systems. *Nature* **197**, 287–289 (1977)
41. Jiang, M., Shen, Y., Jian, J., Liao, X.: Stability, bifurcation and a new chaos in the logistic differential equation with delay. *Phys. Lett. A* **350**, 221–227 (2006)
42. Vasegh, N., Sedigh, K.: Delayed feedback control of dime-delayed chaotic systems: analytical approach at Hopf bifurcation. *Phys. Lett. A* **372**, 5110–5114 (2008)